THE PENNSYLVANIA STATE UNIVERSITY
SCHREYER HONORS COLLEGE

DEPARTMENT OF AEROSPACE ENGINEERING

A Viscous-Inviscid Channel Flow Approach for Preliminary Wind Tunnel Design

JOHN BOERCHERS
SPRING 2022

A thesis
submitted in partial fulfillment
of the requirements
for a baccalaureate degree
in Aerospace Engineering
with honors in Aerospace Engineering

Reviewed and approved* by the following:

David K. Hall
Assistant Professor of Aerospace Engineering
Thesis Supervisor

Mark D. Maughmer
Professor of Aerospace Engineering
Honors Adviser

* Electronic approvals are on file.

ABSTRACT

This thesis will present the development of a quasi-one-dimensional, viscous-inviscid approach to assess the aerodynamic performance of low-speed wind tunnels and its application to the preliminary design of a new wind tunnel. The approach includes numerical integration of the incompressible, quasi-one-dimensional equations of motion coupled with the axisymmetric integral boundary layer equations. The boundary layer model describes the viscous losses necessary for predicting required fan input power. Components such as screens and fans are modeled with discrete changes in the flow variables at specified locations. The approach can be used to assess the aerodynamic performance of a given wind tunnel design to determine the required fan input to overcome viscous losses from the boundary layer and components. Results are provided for the conceptual design of a low-speed wind tunnel for testing turbomachinery. For a fan diameter of 24 inches, a diffuser area ratio of 1.06 provides the maximum test Reynolds number for a 300-horsepower constraint. The results show the utility of the approach for preliminary aerodynamic analysis and design of low-speed wind tunnel designs, enabling rapid design iterations for new wind tunnel designs and assessment of potential design improvements for existing wind tunnels.

TABLE OF CONTENTS

LIST OF FIGURES

LIST OF TABLES

NOMENCLATURE

A = cross-sectional area
AR = area ratio
b = boundary layer lateral width parameter
$\overline{b}$ = non-dimensional boundary layer lateral width parameter, b/L_{ref}
b_o = cross section perimeter
$c_{\mathcal{D}}$ = dissipation coefficient, $\mathcal{D}/\rho_e u_e^3$
c_f = skin friction coefficient, $\tau_w/(1/2\,\rho u^2)$
c_p = pressure coefficient, $p - p_{ref}/\left(1/2\,\rho \mathrm{u}_{\mathrm{ref}}^2\right)$
c_{p_t} = total pressure coefficient, $p_t - p_{ref}/\left(1/2\,\rho \mathrm{u}_{\mathrm{ref}}^2\right)$
c_P = power coefficient, $P/(\dot{m}u^2)$
c_z = absolute axial velocity
c_θ = absolute tangential velocity
$\mathcal{D}$ = dissipation integral, $\int_0^{n_e} \tau(\partial u/\partial n)dn$
H = shape factor, δ^*/θ
H^* = kinetic energy shape factor, θ^*/θ
H^{**} = density flux shape factor
h_t = total enthalpy
K = screen *k*-value
L = length
M_e = edge Mach number
$\dot{m}$ = channel mass flow, $\rho u A$
$\dot{m}_i$ = equivalent inviscid mass flow, $\rho_e u_e A_e$
n = normal spatial coordinate
P = power
p = pressure
p_t = total pressure
R = radius from fan hub
Re = Reynolds number, uL/ν
Re_θ = Reynolds number based on momentum thickness, $u\theta/\nu$
s = spatial coordinate aligned with mean flow
s_o = initial spatial location
$\mathcal{s}$ = entropy
T = temperature
U = shaft tangential velocity, ΩR
u = channel velocity

$\bar{u}_e$ = non-dimensional velocity, u_e/u_{ref}
α = absolute angle
β = relative angle
δ^* = displacement thickness, $\int_0^{n_e}(1-\rho u/\rho_e u_e)dn$
$\bar{\delta}^*$ = non-dimensional displacement thickness, δ^*/L_{ref}
θ = momentum thickness, $\int_0^{n_e}(1-u/u_e)\,\rho u/\rho_e u_e\,dn$
θ^* = kinetic energy thickness, $\int_0^{n_e}(1-u^2/{u_e}^2)\,\rho u/\rho_e u_e\,dn$
$\bar{\theta}$ = non-dimensional momentum thickness, θ/L_{ref}
$\bar{\theta}^*$ = non-dimensional kinetic energy thickness, θ^*/L_{ref}
μ = fluid dynamic viscosity
ν = fluid kinematic viscosity
ρ = fluid density
τ_w = wall shear stress, $\mu(\partial u/\partial n|_{n=0})$
ϕ = flow coefficient, $c_z/\Omega R$
ψ = stagnation pressure rise coefficient, $\Delta p_t/\rho U^2$
Ω = shaft angular velocity

Subscripts

diff = diffuser
e = boundary layer edge
ref = reference
w = wall

ACKNOWLEDGEMENTS

Seeing this work as a culmination of my undergraduate career at Penn State, I would like to take this opportunity to extend my warmest thanks to those who have helped me along the way. Of course, I must begin by thanking Dr. Hall, who served not only as my thesis advisor, but also as a mentor over the course of our time together. Dr. Hall's dedication to his students is remarkable, and I am incredibly grateful to have had the opportunity to learn from him. Additionally, I want to thank Dr. Maughmer for serving as my honors advisor and reader for this thesis.

I would also like to take this opportunity to thank everyone who supported me during my undergraduate career: most notably my friends and family. Without the endless support from my parents and brothers, I would not have made it this far. Specifically, I would like to thank my father who, by example, has taught me a thing or two about perseverance this last year. And finally, I want to thank my partner, Megan, for everything she has done for me these last four years (which included spending countless nights at the library during the writing of this thesis). This achievement is as much hers as it is mine.

Chapter 1

Introduction

Wind tunnel testing remains a fundamental contributor to the success of any aerospace design. Even with the rapid growth and advancement of computational fluid dynamics (CFD) over the last several decades, wind tunnels continue to play an important role in any quality aerodynamic analysis – especially in combination with computational methods. With the ubiquitous usage of wind tunnels, their design process is well-documented, for example in references [1-2], which detail the design of low-speed wind tunnels with Mach numbers less than approximately 0.3 such that the flow can be treated as incompressible.

The conceptual phase of the design process seeks to find the high-level, desirable characteristics of the design. For wind tunnels, this might include basic geometric parameters, such as the test section cross-sectional area and velocity, overall footprint of the tunnel, and power requirements. At this stage, a full three-dimensional CFD solver is not advantageous, partially because it provides more information than necessary for initial comparison and insight and also because no detailed description of the geometry exists yet. In this thesis, a quasi-one-dimensional, viscous-inviscid flow model is developed for use in the early stages of wind tunnel design by quickly and efficiently evaluating new designs.

The approach developed in this thesis were motivated by the goal to develop a new wind tunnel for assessing turbomachinery response to non-uniform inlet flows, such as those encountered in boundary layer ingesting (BLI) propulsion systems. Previous work showed a 9% reduction in mechanical flow power as a result of BLI [3], however other work suggests the non-

uniform inlet flow may reduce the fan efficiency η_{fan} by up to 6% for propulsors designed for uniform inlet flows [4], reducing the overall benefit of BLI. These results suggest a need for a fan design for non-uniform inlet flows with a higher fan efficiency η_{fan} to enable the benefit of BLI. To investigate this, the wind tunnel design will assess the performance of a single stage fan using distortion screens capable of generating non-uniform inlet flows representative of BLI velocity profiles. Although the approach is applied to the preliminary design of the tunnel described, the method is meant to be applicable to general wind tunnel design regardless of the size, architecture, or application.

The thesis is organized as follows: Chapter 2 introduces the quasi-one-dimensional channel flow description, the governing equations for the inviscid and viscous models, and explains the method for incorporating screen and fan models and their effects on the flow within the tunnel. Chapter 3 details the numerical solution approach. Chapter 4 applies the solver to a canonical wind tunnel design and exploration of the design space for the conceptual design of the tunnel. The results of Chapter 4 indicate a diffuser area ratio of 1.06 maximizes the test Reynolds number for a wind tunnel with a 24-inch fan and total 300-horsepower constraint. Chapter 5 provides a summary, the key conclusions, and suggestions for future work.

Chapter 2

Quasi-One-Dimensional Channel Description

2.1 Modeling the Flow

The internal flow analysis is built on a *quasi-one-dimensional* flow description. Within a wind tunnel, the flow field is three-dimensional, with velocity components and gradients in each spatial dimension. For a well-designed wind tunnel however, the most significant velocity component is aligned with the mean flow direction, and the quasi-one-dimensional description is an appropriate approximation. Details of the quasi-one-dimensional flow description are provided in numerous references, including [5], [6], and [7].

The model can be further segmented into two distinct approaches: one model which is entirely inviscid and the other which incorporates the effects of viscosity. Although, the inviscid model cannot provide insight into viscous phenomena such as flow separation or viscous losses in the boundary layer, it serves several important purposes in the early design phase. Most importantly, the inviscid governing equations can be solved *algebraically*. Even without viscous effects, the inviscid flow description relates geometry, pressure, and velocity, providing initial insight into a design's aerodynamic performance. For high Reynolds numbers, where the effects of viscosity become less appreciable compared to the inertial effects, the inviscid model can be a useful first approximation of the tunnel velocity and pressure field.

The quasi-one-dimensional flow description can be extended to include the effects of viscosity by coupling an inviscid quasi-one-dimensional core flow to an axisymmetric integral boundary layer model.

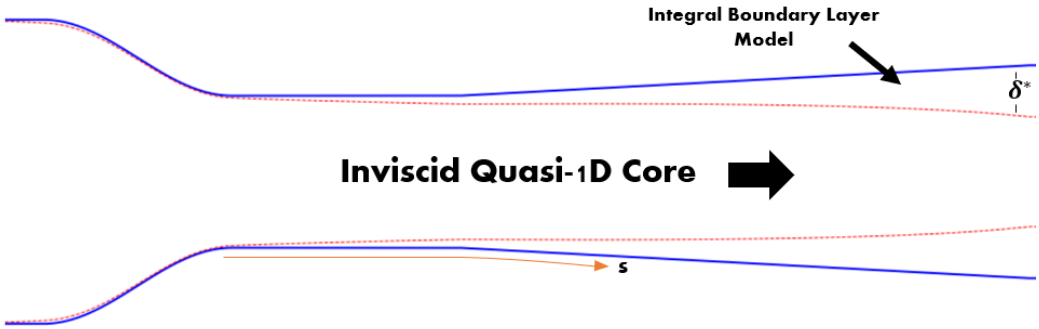

Figure 1. Inviscid Quasi 1D Core with Integral Boundary Layer

The viscous model allows the designer insight into important viscous phenomena such as flow separation and losses to the viscous dissipation which must be overcome with additional fan power.

2.2 Governing Equations

In this section, we develop the equations of motion for incompressible channel flow. Descriptions are provided for each case: inviscid and viscous channel flow.

2.2.1 Inviscid Channel Flow

For the inviscid, incompressible, steady, quasi-one-dimensional case, the equations of motion are simple and can be solved algebraically. Mass conservation requires the mass flux $\dot{m}$ to be constant along the channel,

$$\frac{d\dot{m}}{ds} = \frac{d}{ds}[\rho u A] = 0. \quad (1)$$

In eq. (1), s is the spatial coordinate aligned with the mean flow, ρ is the fluid density, u is the fluid velocity, and A is wind tunnel cross-sectional area. For an incompressible flow, density, ρ, is uniform. The tunnel geometry serves as an input, and so the area $A(s)$ is known at each location. The velocity can thus be determined at each location by using eq. (1),

$$\left(\frac{u}{u_{\text{ref}}}\right) = \left(\frac{A}{A_{\text{ref}}}\right)^{-1}. \quad (2)$$

The velocity profile can then be used to calculate the pressure profile throughout the tunnel. For adiabatic flow, with no work done on or by the flow, and no entropy generation, the stagnation pressure, p_t, is constant and equal to the ambient pressure, p_∞, assuming the source of the flow for an open-circuit wind tunnel is static, ambient air, and can be expressed using Bernoulli's equation,

$$p + \frac{1}{2}\rho u^2 = p_t. \quad (3)$$

To make the problem non-dimensional, a pressure coefficient, c_p, is introduced,

$$c_p = \frac{p - p_\infty}{\frac{1}{2}\rho u_{ref}^2}. \quad (4)$$

The tunnel inlet velocity serves as the reference velocity, u_{ref} in this method, which will be elaborated on further in the numerical approach. The addition of components into the channel, however, will change the total pressure of the flow, c_{p_t}; for example, a fan will do work on the flow field and, consequently, increase the total pressure of the flow,

$$c_{p_t} = \frac{p_t - p_\infty}{\frac{1}{2}\rho u_{ref}^2}. \quad (5)$$

Combining eqs. (3), (4), and (5) yields the non-dimensional result,

$$c_p = c_{p_t} - \left(\frac{u}{u_{ref}}\right)^2 . \tag{6}$$

Eqs. (2) and (6) can be solved algebraically for $\frac{u}{u_{ref}}$ and c_p provided a given $\frac{A}{A_{ref}}$ vs s distribution with discrete total pressure changes Δc_{p_t} at components, discussed further in Chapter 3.

2.2.2 Viscous Channel Flow

The viscous channel flow requires the addition of several boundary layer parameters, which, in turn, requires additional relations to close the system. The governing equations still rely on the principles of conservation of mass and momentum; however, two additional equations are needed to account for the blockage effect due to the growth of the boundary layer (kinematic) and boundary layer dissipation (conversation of energy).

Integral boundary layer parameters abstract away the details of the boundary layer flow via integration in the normal direction, yielding a one-dimensional description of the boundary layer, which is coupled to the quasi-one-dimensional, inviscid flow. Below, we review relevant parameters that appear in the viscous equations of motion which follow. A more complete description is provided by Schlicting [8] and Drela [9].

The displacement thickness, δ^*, describes mass flow reduction due to the boundary layer blockage,

$$\delta^* = \int_0^{n_e} \left(1 - \frac{\rho u}{\rho_e u_e}\right) dn . \tag{7}$$

The velocity profile would be uniform, u_e, throughout the area defined by the normal length, n_e, with a mass flow, $\dot{m}_i$, if the flow were entirely inviscid.

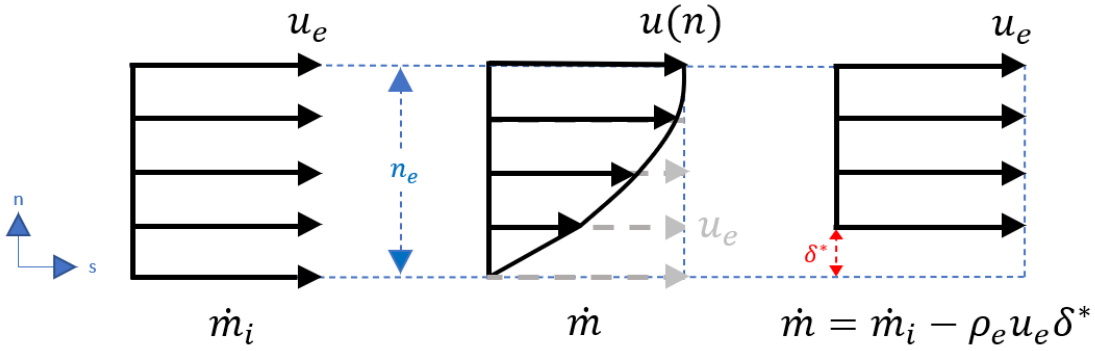

Figure 2. Comparison of Inviscid and Boundary Layer Velocity Profiles

The viscous shearing and no slip condition at the wall distorts the velocity to resemble a profile $u(n)$, similar to the middle profile in Figure 2, with a reduced mass flow $\dot{m}$ in the area defined by n_e, the normal extent over which $u(n)$ is less than the boundary layer edge velocity u_e. The *mass defect* $\rho_e u_e \delta^*$ is the difference between the mass flows $\dot{m}_i - \dot{m}$ in the area defined by n_e, such that the mass defect height is the displacement thickness δ^* found using eq. (7). The displacement thickness δ^* can be interpreted as the change in height needed to describe the flow as inviscid with the same mass flow $\dot{m}$ as the viscous case. This effect of decreasing the passage area for the inviscid core flow generates a blockage effect. See reference [9] for more information.

The boundary layer momentum thickness θ is defined by eq. (8),

$$\theta = \int_0^{n_e} \left(1 - \frac{u}{u_e}\right) \frac{\rho u}{\rho_e u_e} dn. \tag{8}$$

The *momentum defect* $\rho_e u_e^2 \theta$ describes the difference in momentum flux between the viscous boundary layer and inviscid ($u = u_e$) flow with the same mass flow $\dot{m}$.

The shape factor, *H*, relates the momentum and displacement thicknesses,

$$H = \frac{\delta^*}{\theta}. \tag{9}$$

H increases as the boundary layer approaches separation [9], and it therefore provides insight into the 'health' of the boundary layer when analyzing the results for a given wind tunnel design.

The kinetic energy thickness θ^* is found by integrating the difference in the kinetic energy fluxes for the inviscid and viscous cases across the boundary layer, similar to the previous calculations for mass and momentum flux,

$$\theta^* = \int_0^{n_e} \left(1 - \frac{u^2}{{u_e}^2}\right) \frac{\rho u}{\rho_e u_e} dn. \tag{10}$$

The *kinetic energy defect* $\frac{1}{2}\rho_e u_e^3 \theta^*$ is a measure of the rate at which energy is dissipated through the viscous action in the boundary layer making it a parameter of interest for wind tunnel design because this lost power must be overcome by additional fan power.

The kinetic energy shape factor H^*, relates the kinetic energy thickness θ^* to the momentum thickness θ,

$$H^* = \frac{\theta^*}{\theta}. \tag{11}$$

With these parameters, the governing equations for the viscous case are now introduced. Mass conservation must now include the effective area reduction from the growth of the boundary layer, as described by the boundary layer lateral width parameter,

$$b = b_o - 2\pi\delta^*. \tag{12}$$

In eq. (12), b_o is the perimeter of the tunnel path without the boundary layer, and b is the perimeter of the path reduced by the growth of the boundary layer.

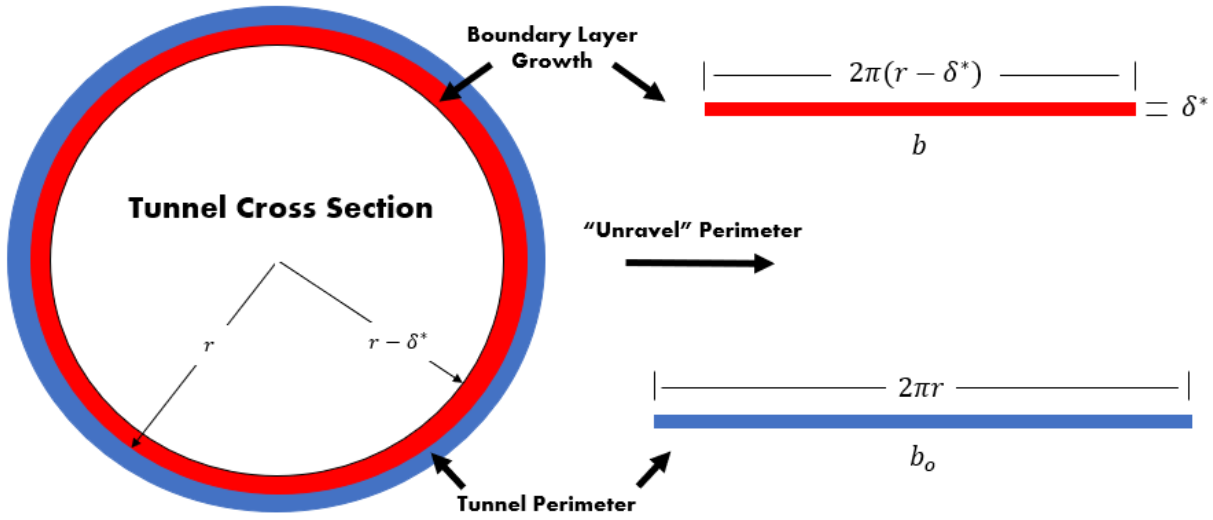

Figure 3. Boundary Layer Lateral Width Parameter

The conservation of mass differs from the inviscid case by the inclusion of the boundary layer mass defect which reduces the area of the core flow,

$$\frac{d\dot{m}}{ds} = \frac{d}{ds}[\rho u(A - b\delta^*)] = 0. \tag{13}$$

The integral boundary layer model employs the Thin Shear Layer (TSL) approximations. That is, for a flow where the characteristic axial length is much greater than the characteristic boundary layer height – and the resulting normal gradients far greater than their axial counterparts – the TSL equations are readily reduced to their integral forms which incorporate the previously described boundary layer parameters. Application of TSL yields ordinary differential equations for boundary layer conservation of momentum and energy in terms of the integral metric described above [9]:

$$\frac{d\theta}{ds} = \frac{c_f}{2} - (H + 2 - M_e^2)\frac{\theta}{u_e}\frac{du_e}{ds} - \frac{\theta}{b}\frac{db}{ds} \tag{14}$$

$$\frac{d\theta^*}{ds} = 2c_{\mathcal{D}} - \left(2\frac{H^{**}}{H} + 3 - M_e^2\right)\frac{\theta^*}{u_e}\frac{du_e}{ds} - \frac{\theta^*}{b}\frac{db}{ds}. \tag{15}$$

Eq. (14) is the non-dimensional Von Karman Integral Momentum Equation including a term to extend the analysis to an axisymmetric flow by accounting for the boundary layer lateral width parameter b. Eq. (15) combines the Von Karman Integral Momentum Equation with the boundary layer conservation of energy. These equations are simplified for the incompressible case where the edge Mach number, ${M_e}^2$, and the density flux shape parameter, H^{**}, may be neglected. Under these assumptions, eq. (14) can be expressed as,

$$\frac{d}{ds}(\theta b) = b\frac{c_f}{2} - (H + 2)\frac{\theta b}{u_e}\frac{du_e}{ds}. \tag{16}$$

Eq. (16) introduces an additional parameter: the non-dimensional skin friction coefficient $c_f = \tau_w / \frac{1}{2}\rho u^2$, where τ_w is the wall shear stress which is related to the coefficient of viscosity μ and the wall velocity gradient,

$$\tau_w = \mu \left.\frac{\partial u}{\partial n}\right|_{n=0}. \tag{17}$$

For an incompressible flow, eq. (15) can be expressed as,

$$\frac{1}{H^*}\frac{dH^*}{ds} = \frac{2c_{\mathcal{D}}}{\theta H^*} - \frac{c_f}{2\theta} + \frac{(H-1)}{u_e}\frac{du_e}{ds}. \tag{18}$$

Eq. (18) introduces the dissipation coefficient $c_{\mathcal{D}} = \mathcal{D}/\rho_e u_e^3$, where $\mathcal{D}$ is the dissipation integral,

$$\mathcal{D} = \int_0^{n_e} \tau \frac{\partial u}{\partial n} dn. \tag{19}$$

The dissipation coefficient models the rate at which the shear stress dissipates kinetic energy into heat within the flow [9]. Equations (12), (13), (16), and (18) provide the relations necessary to

compute the parameters governing the flow field within the wind tunnel; however, they require a closure model to relate several of the parameters such that the system closes. In the equations of motion, seven variables ($\theta, \theta^*, H, H^*, c_f, c_{\mathcal{D}}$, and b) are unknown. To solve the four equations of motion, three closure relations are required.

2.3 Turbulent Boundary Layer Closure

It is assumed that the wind tunnel Reynolds number is sufficiently high such that the boundary layer is turbulent. Since no form of the wall shear stress τ_w is assumed in the derivation of the equations of motion, the equations may also apply for time-averaged turbulent flows [7]. The turbulent closure relations from [10] are used to relate the kinetic energy shape factor H^*, skin friction coefficient c_f, and dissipation coefficient $c_{\mathcal{D}}$, to the shape factor H and the momentum thickness Reynolds number for a turbulent boundary layer,

$$H^*(H) = \begin{cases} 1.509 + 0.1642\dfrac{(4-H)^{1.6}}{H}, & \text{if } H < 4 \\ 1.509 + (H-4)^2\left[\dfrac{0.04}{H} + \dfrac{0.04835}{(H-4.579)^2}\right], & \text{if } H > 4 \end{cases} \tag{20}$$

$$c_f(H, Re_\theta) = 0.3e^{-.133H}(\log_{10}\mathrm{Re}_\theta)^{-1.74-0.31H} + 0.00011\left[\tanh\left(4 - \frac{H}{0.875}\right) - 1\right] \tag{21}$$

$$c_{\mathcal{D}}(H, \mathrm{Re}_\theta) = H^*(H)\left[\frac{c_f(H, \mathrm{Re}_\theta)}{3}\left(\frac{4}{H} - 1\right) + 0.015\left(1 - \frac{1}{H}\right)^3\right] \tag{22}$$

The closure relations require the local Reynolds number based on the momentum thickness, $Re_\theta = {u_e\theta}/{\nu}$.

2.4 Component Modeling

Wind tunnels include different components which assist in achieving the desired aerodynamic performance. For example, almost every wind tunnel requires a fan to provide the power needed to produce the desired test section velocity. Wind tunnels will include screens and turning vanes to condition the flow, suppress separation, and navigate changes of flowpath direction. Closed-circuit wind tunnels may use a heat exchanger to balance the increase in thermal energy from the fan power. Wind tunnel designs can include unique combinations of components necessary for each given application.

In this section we introduce components and describe their effect on the channel flow described in above. The flow parameter variations as a result of the component are modeled as a discrete change in the flow parameters at a specified component location. Models for screens and fans are described in more detail in the following sections. Additional components can be added to the solver in the future provided their effect can be captured and described as a discrete change in flow variables.

2.4.1 Screen Model

Screens are modeled with a *k*-value, that relates the pressure drop through the screen to the dynamic pressure at the screen.

$$\Delta p_{screen} = -\frac{1}{2}\rho u^2 K \tag{23}$$

For incompressible, one-dimensional flows, the pressure drop across a screen or pressure increase across a fan is equivalent to the total pressure change. Conservation of mass is applied across the screen,

$$\rho u^{-} A = \rho u^{+} A, \tag{24}$$

where $u-$ is the velocity before the screen and u^{+} is the velocity downstream of the screen. Since the area A does not change: $u- = u^{+}$. The dynamic pressure is then constant across the screen, so the change in pressure before the screen p^{-} and downstream of the screen p^{+} must be a result of the total pressure drop across the screen Δp_t,

$$p^{-} + \frac{1}{2}\rho u^2 + \Delta p_t = p^{+} + \frac{1}{2}\rho u^2 \tag{25}$$

$$\Delta p_t = p^{+} - p^{-} = \Delta p \tag{26}$$

2.4.2 Fan Model

The test article of interest is an axial fan stage, consisting of a rotating fan rotor followed by stationary exit guide vanes. The pressure rise characteristics of the stage can be modeled at the preliminary design stage using *velocity triangle* analysis [6].

Figure 4 shows the velocity triangles and notation conventions for a fan stage. *c* denotes the velocity with respect to the absolute frame and *ω* denotes the velocity with respect to the frame rotating with the fan stage. The axial velocity component is denoted by c_z and the angles α and β represent the angles from c_z to the absolute and relative velocities respectively. The velocity of the airfoil with respect to the absolute frame U is equivalent to the product of the shaft speed Ω and the radius R. The Kutta Condition requires that the relative velocity exits the airfoil with streamlines parallel to the camberline at the trailing edge, so β_2 is assumed to be constant. For the same c_z, the exiting absolute velocity c_2 and absolute angle α_2 can then be found.

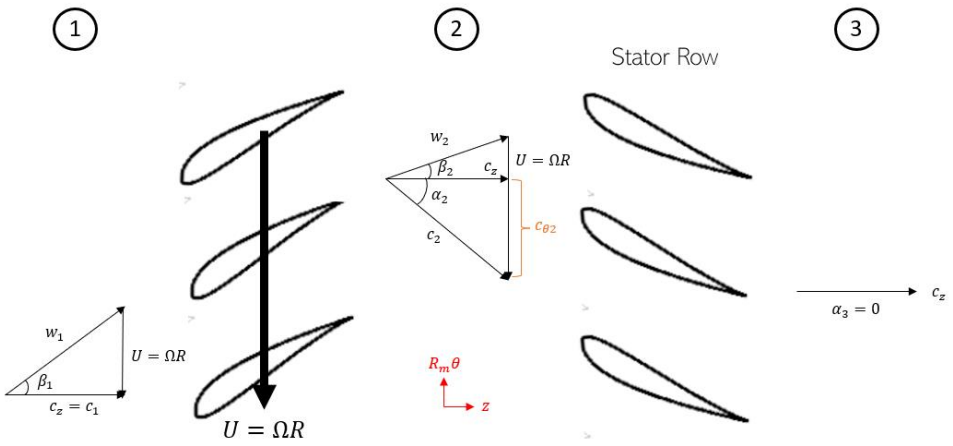

Figure 4. Velocity Triangles for an Ideal Fan Stage

The Euler Turbine equation relates the change in flow velocity to the change in stagnation enthalpy, h_t, across the rotor,

$$\Delta h_t = U(c_{\theta 2} - c_{\theta 1}). \tag{27}$$

Using the velocity triangles displayed in Figure 4, the θ-component of the absolute velocities $c_{\theta 1}$ and $c_{\theta 2}$ can be calculated using the geometry of the velocity triangles,

$$c_{\theta 1} = 0, \tag{28}$$

$$c_{\theta 2} = U - c_z \tan\beta_2. \tag{29}$$

Substituting eqs. (28) and (29) into (27) and dividing by U^2 results in the useful, nondimensional form of the Euler Turbine equation.

$$\frac{\Delta h_t}{U^2} = 1 - \frac{c_z}{U}\tan\beta_2 \tag{30}$$

The non-dimensional pressure rise across the fan $\Delta c_{p_{fan}}$ is needed for wind tunnel performance, and Gibb's equation is used to relate the change in stagnation enthalpy h_t to the change in stagnation pressure Δp_t,

$$T\Delta s = \Delta h_t - \frac{1}{\rho}\Delta p_t. \tag{31}$$

Entropy is denoted with s to differentiate from the spatial coordinate s. For an isentropic process and an incompressible flow, eq. (30) reduces to (31),

$$\Delta h_t = \frac{1}{\rho}\Delta p_t. \tag{32}$$

The non-dimensional groups in eq. (30) are the flow coefficient ϕ ($=\frac{c_z}{U} = \frac{c_z}{\Omega R}$) and the stagnation pressure rise coefficient ψ ($=\frac{\Delta p_t}{\rho U^2} = \frac{\Delta p_t}{\rho(\Omega R)^2}$). Combining eqs. (30), (32), and the non-dimensional flow coefficient, ϕ, and stagnation pressure rise coefficient, ψ,

$$\psi = 1 - \phi \tan\beta_2. \tag{33}$$

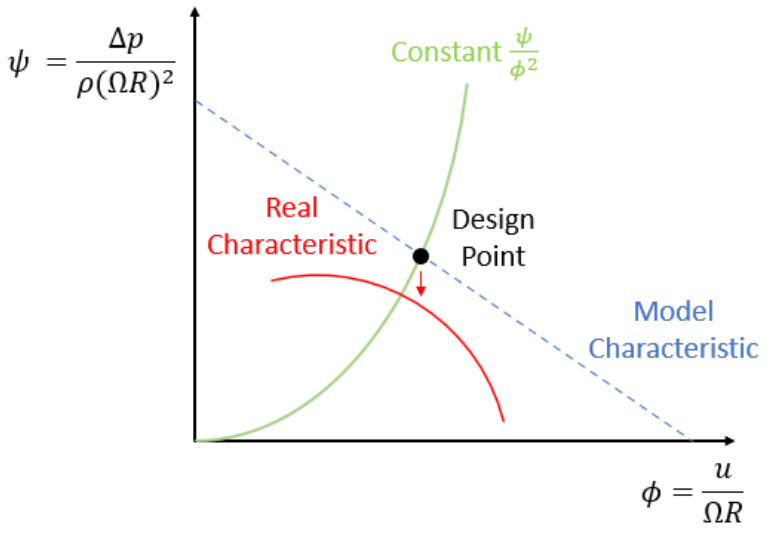

Figure 5. Non-Dimensional Coefficients for Fan Analysis

The result for this case from eq. (33) describes a straight line or the ideal characteristic depicted in blue in Figure 5. As ϕ begins to change the rotor may experiences increased losses due to entropy generation, decreasing the pressure rise coefficient ψ relative to the ideal characteristic. The fan model characteristic is accurate for the design point and can reasonably approximate slight off-design conditions; however, as the flow conditions begin to deviate from the design point, the ideal characteristic begins to vary significantly from the real characteristic, displayed in red in Figure 5.

For the model used in this approach, an ideal fan with the absolute velocity c_1 equal to c_z is used. To acquire the impact of the fan on the wind tunnel performance, it is necessary to relate the design non-dimensional fan parameters to the local velocity $u(= c_z)$ and the fan pressure rise Δp in the following way,

$$\frac{\Delta p_t}{\rho {c_z}^2} = \frac{\Delta p_t}{\rho U^2}\left(\frac{U}{c_z}\right)^2. \tag{34}$$

As mentioned in the previous section, in the incompressible, quasi-one-dimensional model the pressure rise across the fan Δp is equivalent to the increase in stagnation pressure from the fan Δp_t. Recognizing that eq. (34) includes the non-dimensional groups ψ and ϕ and that the axial velocity c_z in this notation is the channel flow velocity u, eq. (35) can be used to relate the design parameters to the change in pressure:

$$\frac{\psi}{\phi^2} = \frac{\Delta p}{\rho u^2} = \frac{\Delta p}{\frac{1}{2}\rho u_{ref}^2}\frac{1}{2}\left(\frac{u_{ref}}{u}\right)^2. \tag{35}$$

Making the result non-dimensional with the reference dynamic pressure $\frac{1}{2}\rho u_{ref}^2$, the change in the non-dimensional pressure coefficient can be calculated across the fan model provided a design work and flow coefficient,

$$\Delta c_{p_{fan}} = 2\left(\frac{\psi}{\phi^2}\right)\left(\frac{u}{u_{ref}}\right)^2. \quad (36)$$

The pressure rise can be related to the power required for the fan. The power is equal to the increase in total enthalpy,

$$P = \dot{m}\Delta h_{\mathrm{t}}. \quad (37)$$

Assuming the axial velocity does not change across the fan and that the fan process is isentropic, eqs. (31) and (37) can be combined and reduced to produce the desired relationship between the pressure rise and power required,

$$P = \dot{m}\frac{\Delta p}{\rho}. \quad (38)$$

Eq. (38) is then rearranged into non-dimensional form and it is found that, for the assumptions stated, the non-dimensional power coefficient c_P is equal to twice the non-dimensional fan pressure rise c_p,

$$c_P = \frac{P}{\dot{m}u_{ref}^2} = \frac{\Delta p}{\rho u_{ref}^2} = 2\Delta c_{p_{fan}}. \quad (39)$$

To summarize, eq. (36) is sufficient to model the design point and implement the effect of the fan on the channel flow. Once the characteristic relating the work coefficient ψ and the flow coefficient ϕ has been established for the wind tunnel and fan design set, the off-design performance can be found using the characteristic. Finally, eq. (39) relates the non-dimensional fan pressure rise, Δc_p, to the non-dimensional power coefficient, c_P.

Chapter 3
Numerical Approach

In this chapter, the governing equations are organized in such a way that they can be readily computed with the solver for the flow parameters.

3.1 Linear System

Eqs. (12), (13), (16), and (18) can be expressed as a system of four ordinary differential equations for the flow field parameters b, u_e, θ, and H,

$$y = \begin{bmatrix} b(s) \\ u_e(s) \\ \theta(s) \\ H(s) \end{bmatrix}. \tag{40}$$

The governing equations can be rearranged into the matrix form $A(y)y' = b(y)$, where the y' vector includes the differential state parameters, the A matrix includes the corresponding coefficients, and the b matrix adds the non-homogeneous terms,

$$\begin{bmatrix} 1 & 0 & 2\pi H & 2\pi\theta \\ \frac{1}{b} & \frac{-1}{u_e}\left(\frac{A}{b\theta H} - 1\right) & \frac{1}{\theta} & \frac{1}{H} \\ \frac{1}{b} & \frac{(H+2)}{u_e} & \frac{1}{\theta} & 0 \\ 0 & \frac{-(H-1)}{u_e} & 0 & \frac{dH^*(H)}{H} \end{bmatrix} \begin{bmatrix} \frac{db}{ds} \\ \frac{du_e}{ds} \\ \frac{d\theta}{ds} \\ \frac{dH}{ds} \end{bmatrix} = \begin{bmatrix} \frac{db_o}{ds} \\ \frac{1}{b\theta H}\frac{dA}{ds} \\ \frac{c_f(u,\theta,H)}{2\theta} \\ \frac{2c_{\mathcal{D}}(u,\theta,H)}{\theta H^*(H)} - \frac{c_f(u,\theta,H)}{2\theta} \end{bmatrix}. \tag{41}$$

The channel flow can thus be solved as an initial value problem (IVP), and then the solution is found by integrating forward in *s* from the condition at the inlet.

3.2 Non-Dimensional Forms of the Viscous Governing Equations

The inlet diameter, $L_{ref} = 2r(s_o)$, and velocity, $u_{ref} = u(s_o)$, serve as the dimensional reference scale for the problem because the governing differential equations comprise an IVP. Thus, the parameters in eqs. (41) are made non-dimensional by the appropriate reference and expressed as $\bar{u}_e$, $\bar{b}$, $\bar{\delta}^*$, $\bar{\theta}$, $\bar{\theta}^*$, and $\bar{s}$ where $\bar{u}_e = \frac{u_e}{u_{ref}}$, $\bar{b} = \frac{b}{L_{ref}}$, $\bar{\delta}^* = \frac{\delta^*}{L_{ref}}$, $\bar{\theta} = \frac{\theta}{L_{ref}}$, and $\bar{\theta}^* = \frac{\theta^*}{L_{ref}}$,

$$\begin{bmatrix} 1 & 0 & 2\pi H & 2\pi\bar{\theta} \\ \frac{1}{\bar{b}} & \frac{-1}{\bar{u}_e}\left(\frac{\bar{A}}{\bar{b}\bar{\theta}H} - 1\right) & \frac{1}{\bar{\theta}} & \frac{1}{H} \\ \frac{1}{\bar{b}} & \frac{(H+2)}{\bar{u}_e} & \frac{1}{\bar{\theta}} & 0 \\ 0 & \frac{-(H-1)}{\bar{u}_e} & 0 & \frac{dH^*(H)}{H} \end{bmatrix} \begin{bmatrix} \frac{d\bar{b}}{d\bar{s}} \\ \frac{d\bar{u}_e}{d\bar{s}} \\ \frac{d\bar{\theta}}{d\bar{s}} \\ \frac{dH}{d\bar{s}} \end{bmatrix} = \begin{bmatrix} \frac{d\bar{b}_o}{d\bar{s}} \\ \frac{1}{\bar{b}\bar{\theta}H}\frac{d\bar{A}}{d\bar{s}} \\ \frac{c_f(\bar{u}, \bar{\theta}, H)}{2\theta} \\ \frac{2c_{\mathcal{D}}(\bar{u}, \bar{\theta}, H)}{\bar{\theta}H^*(H)} - \frac{c_f(\bar{u}, \bar{\theta}, H)}{2\bar{\theta}} \end{bmatrix}. \quad (42)$$

3.3 Inlet Conditions

The inlet conditions first need to be specified to solve the IVP. The inlet is meant to represent the behavior of flow in a bell mouth inlet, with boundary layer acceleration from a stagnation point. H is initialized to 1.3, corresponding to a turbulent boundary layer with zero pressure gradient [8].

A reference Reynolds number at the inlet Re_{ref} is also specified. The momentum thickness Reynolds number Re_θ at the inlet governs the initial momentum thickness $\theta(s_o)$,

$$\frac{\theta(s_o)}{L_{ref}} = \frac{\nu Re_\theta(s_o)}{L_{ref}u(s_o)} = \frac{Re_\theta(s_o)}{Re_{ref}}. \quad (43)$$

In the numerical model the momentum thickness at the inlet $\theta(s_o)$ is made as small as possible. The turbulent closure relations described in Chapter 2, however, rely on the momentum

thickness Reynolds number Re_θ to compute the dissipation coefficient $c_\mathcal{D}$ and the skin friction coefficient c_f, which are undefined for $\theta = 0$. Test cases were run where Re_θ was iteratively reduced in the solver until the domain issue was encountered.

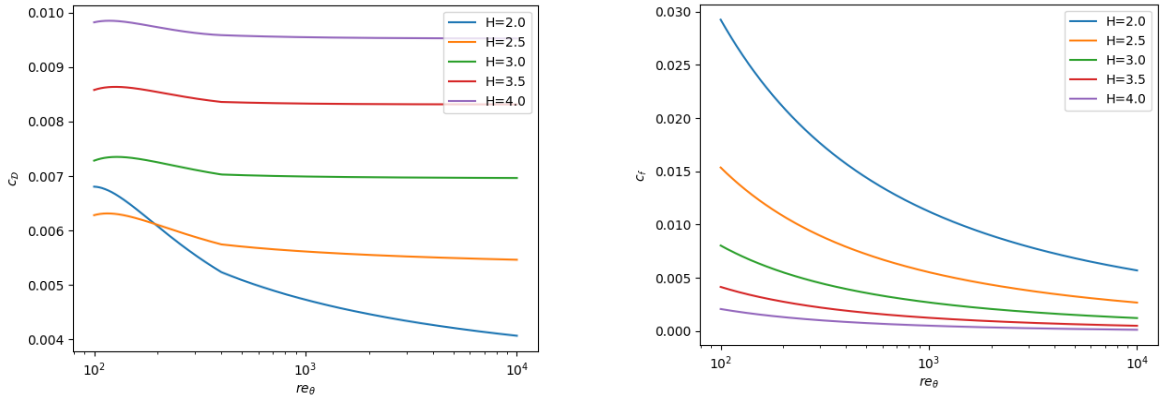

Figure 6. Dissipation and Skin Friction Coefficients at Low Momentum Thickness Reynolds Numbers

It was found that setting Re_θ to 250 at the inlet served as the lowest value which could be set before the onset of the numerical issues. The inlet $\bar{\theta}$ is therefore set to $\frac{\theta(s_o)}{L_{ref}} = \frac{250}{Re_{ref}}$.

Knowing the initial shape parameter $H(s_o)$ and momentum thickness $\theta(s_o)$, the initial boundary layer lateral width parameter $b(s_o)$ can be calculated based on the geometry described in Figure 3,

$$\frac{b(s_o)}{L_{ref}} = 2\pi\left(\frac{r(s_o)}{L_{ref}} - \frac{\theta(s_o)}{L_{ref}}H(s_o)\right). \tag{44}$$

Since the inlet diameter serves as the reference length, the value $\frac{r(s_o)}{L_{ref}}$ is equal to 0.5 in the computation for the initial boundary layer lateral width parameter $b(s_o)$.

The non-dimensional velocity $\bar{u}_e$ at the inlet equals 1 since the inlet velocity serves as the reference velocity. With this, the four parameters each have an initial value,

$$\begin{bmatrix} \bar{b}(s_o) \\ \bar{u}(s_o) \\ \bar{\theta}(s_o) \\ H(s_o) \end{bmatrix} = \begin{bmatrix} 2\pi\left(\frac{r(s_o)}{L_{ref}} - \frac{\theta(s_o)}{L_{ref}}H(s_o)\right) \\ 1 \\ 250/Re_{ref} \\ 1.3 \end{bmatrix}. \tag{45}$$

3.4 Implementation

The Python SciPy function, solve_ivp [11] was used with the fifth-order, explicit Runge-Kutta method, RK45 [12][13] to integrate eq. (42). The code allowed for the inclusion of components at specified s locations and would then integrate in s between the components using solve_ivp, implement the component transfer functions described in Section 2.4, and repeat the process until the integration reached the end of the wind tunnel domain.

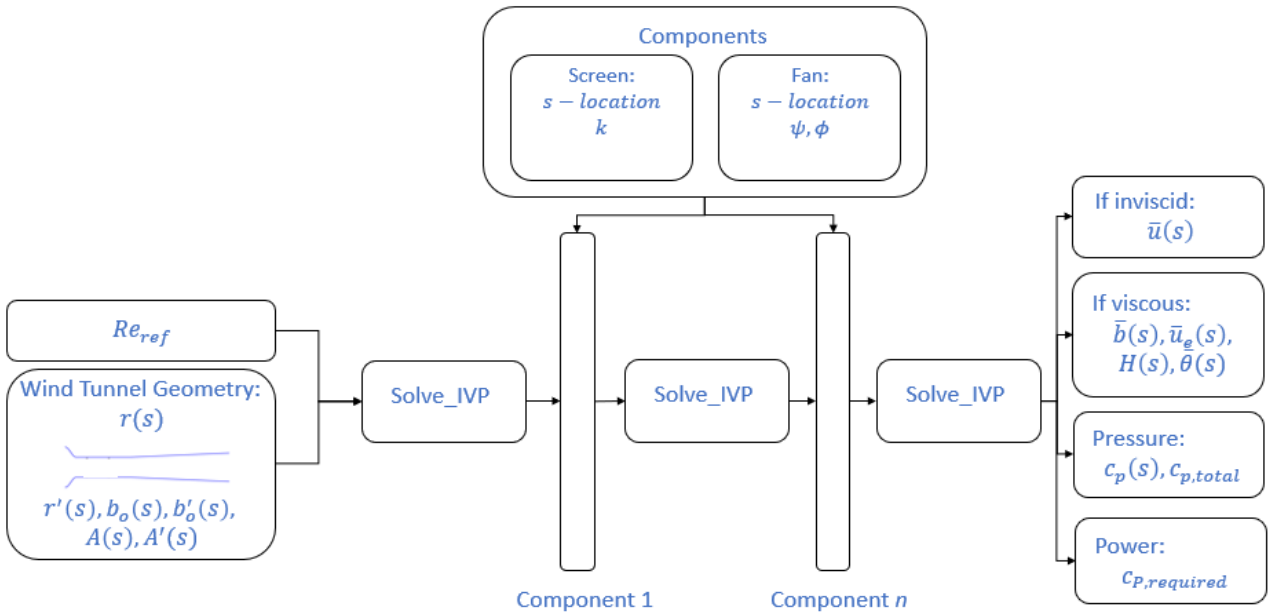

Figure 7. Solver Block Diagram

3.5. Grid Convergence

This section illustrates the grid convergence study for the notional wind tunnel design presented in Chapter 4 to ensure convergence in the results. Solve_ivp sets the grid spacing such that it achieves numerical stability, however, a grid convergence study was performed for a representative tunnel design by specifying a maximum step size to assure convergence of flow variables. To verify convergence, the non-dimensional pressure rise across the test fan $c_{p_{test\ fan}}$ for the viscous and inviscid cases were compared for maximum step sizes ranging from 1 to 10^{-4} times L_{total}. Below a step size of $0.01L_{\text{total}}$, the non-dimensional pressure coefficient c_p does not change for the viscous and inviscid case, and the grid sizing is considered converged.

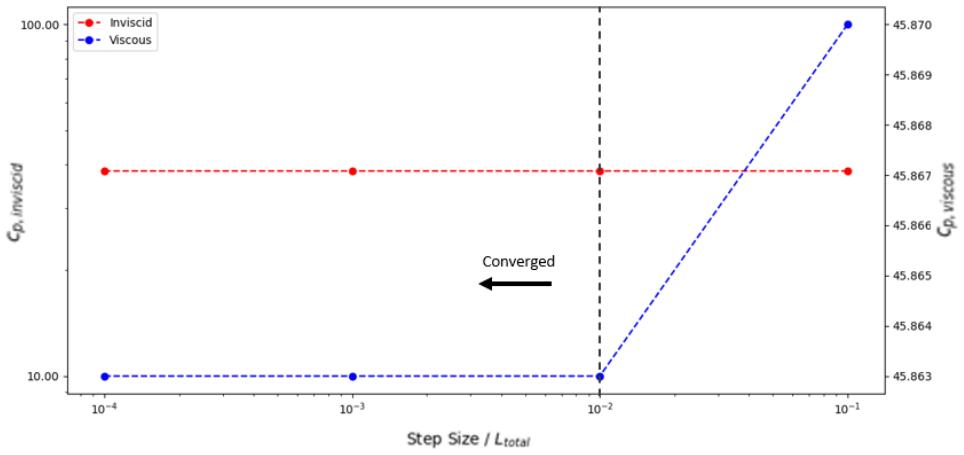

Figure 8. Grid Convergence for Varying Step Sizes

The inviscid pressure coefficient converges for a step size of $0.1L_{\text{total}}$ since the problem is algebraic. A greater step size will increase computation speed, so the following analyses utilize the $0.01L_{\text{total}}$ step size; the greatest step size which still results in convergence for both cases.

Chapter 4

Conceptual Wind Tunnel Design

In this chapter the approach described in Chapters 2-3 is applied to the conceptual design of a wind tunnel for testing fan performance. The first section presents the methodology for parameterizing the design space. The second section presents the results for a notional wind tunnel design. Finally, the third section demonstrates preliminary wind tunnel design by using the solver to identify parameters which produce desirable performance.

4.1 Parameterizing the Design Space

The tunnel geometry is described parametrically by the fan diameter d_{fan}, diffuser area ratio AR_{diff}, and the total length $L_{t\text{otal}}$. A distortion screen creates a flow field which varies in the normal direction across the cross section of the wind tunnel. To capture this effect in the quasi-one-dimensional model, a screen *k*-value of 0.5 is used for an average pressure drop across the screen. A test fan is modeled as an ideal fan with a pressure rise coefficient, ψ, 0.3 and a flow coefficient, ϕ, 0.5. If the pressure coefficient is below zero at the end of the wind tunnel length, the blower fan at the exit provides the power needed to induce flow through the tunnel and overcome viscous losses; the power required for these fans is one of the results of interest. Otherwise, if the pressure coefficient is above zero at the end of the wind tunnel, then a throttle returns the pressure coefficient to zero.

The total length of the tunnel L_{total} is specified to represent the footprint constraint of the wind tunnel facility. To avoid component interactions, one half of the fan diameter $\frac{d_{\text{fan}}}{2}$ separates

the contraction from the screen, one fan diameter d_{fan} separates the screen from the test fan, and one fan diameter separates the test fan from the beginning of the diffuser section (see Figure 9). The test section, from the end of the inlet contraction to the start of the diffuser, is constant area equal to πd_{fan}^2

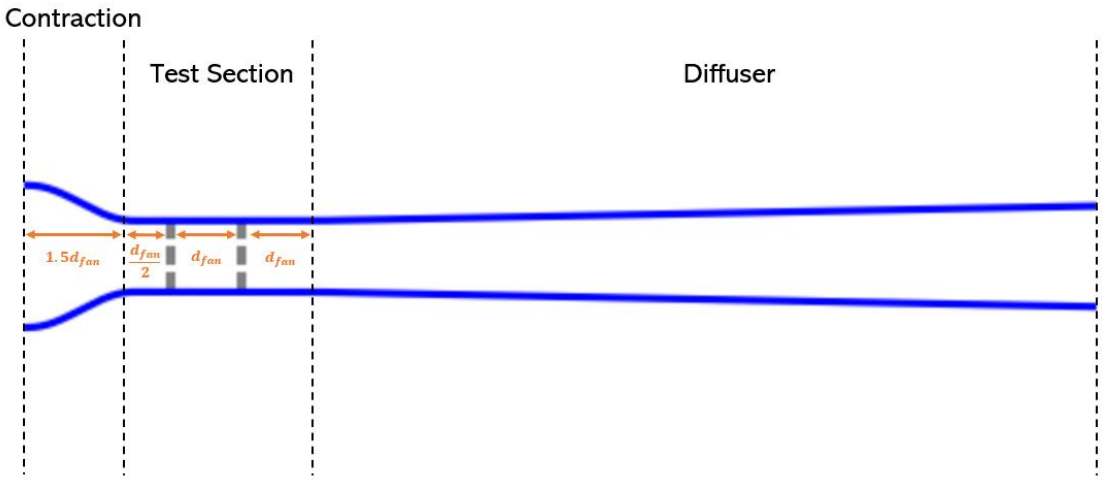

Figure 9. Sections of Example Tunnel Geometry

The maximum length of the diffuser, L_{diff}, is then the difference in the total length, L_{total}, and the combined length of the contraction and test section which is equal to $4d_{\text{fan}}$,

$$L_{\text{diff}} = L_{\text{total}} - 4d_{\text{fan}}. \tag{46}$$

The diffuser wall radius varies linearly with s. The diffuser area ratio AR_{diff} specifies the ratio of the diffuser exit area to the test section area. The area ratio of the inlet contraction area to test section area AR_{contr} is set to a default value, in this case that value is 2. The variation in radius through the contraction is modeled with a half-cosine curve. The dimensional description of the tunnel geometry is made non-dimensional using the reference length L_{ref}, the inlet diameter.

4.2 Example Design

This section provides an in-depth look at the results of the approach applied to a design, illustrating the capabilities of the solver. Table 1 lists the geometric parameters for a notional tunnel geometry. A test fan with diameter 24 inches and a diffuser area ratio of 1.25 are used.

Table 1. Example Tunnel Geometry Characteristics

Fan diameter $d_{\mathbf{fan}}$	0.601 meters (24 inches)
Diffuser Area Ratio $AR_{\mathbf{diff}}$	1.25
Total Tunnel Length $L_{\mathbf{total}}$	9.14 meters (30 feet)
Diffuser Length $L_{\mathbf{diff}}$	6.73 meters (22.1 feet)

With the tunnel geometry defined, the final parameter, the reference Reynolds number Re_{ref}, describes the magnitude of the velocity through the tunnel. For this example, Re_{ref} was set to 1 million such that $u_{inlet} = 12.1\ m/s$ and $u_{test} = 48.6\ m/s$ for air.

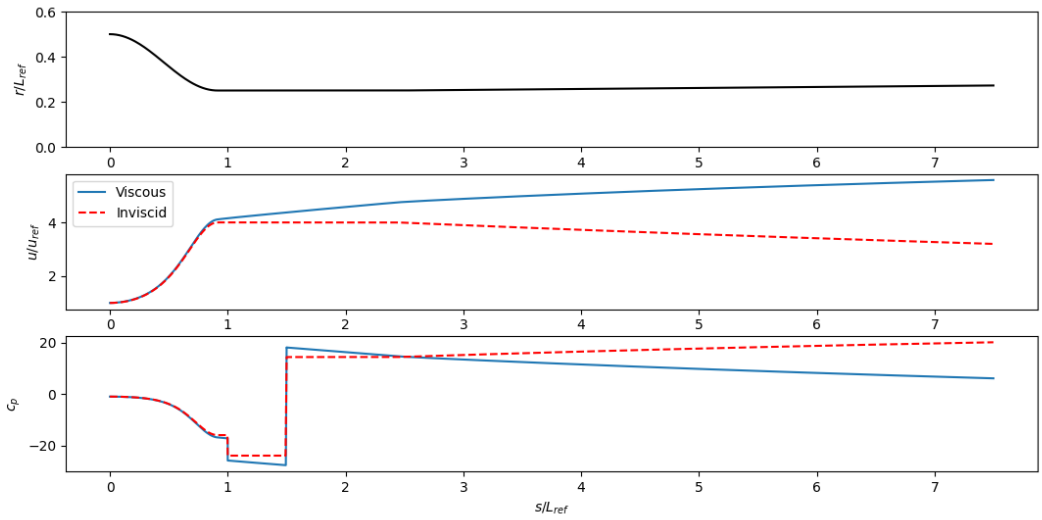

Figure 10. Velocity and Pressure Profiles in Example Design

The tunnel geometry, velocity, and pressure profiles are shown in Figure 10 for the inviscid and viscous cases. In the inviscid profile, the velocity is constant in the test section where the tunnel area is not changing. However, in the viscous profile, the velocity increases as the boundary layer displacement thickness increases. When the test fan provides a pressure rise which raises the non-dimensional pressure coefficient above zero, it can be beneficial to use a diffuser area ratio below 1, a nozzle, to reduce the pressure before a throttle at the exit. In the notional design presented here, the blockage in the diffuser overcomes the deceleration from the diffuser and acts as a nozzle, accelerating the flow and reducing the pressure.

Additionally in Figure 10, the non-dimensional pressure coefficient c_p profiles are plotted along the tunnel. The discrete changes in c_p are a result of the pressure change across the screen and fan. The inviscid case does not model the losses to viscous dissipation in the boundary layer, and so the inviscid pressure coefficient c_p does not change in the constant area test section, while the viscous c_p continues to decrease due to the blockage effect. The exit throttle must return the pressure coefficient c_p to zero. The total power coefficient, $c_{P,\text{total}}$, describing the power requirements of the system is twice the test fan pressure coefficient $c_{p,\text{test fan}}$. If the pressure coefficient were still below zero at the exit, the total power coefficient would be twice the sum of the fan pressure coefficient, $c_{p,\text{test fan}}$, and the blower fan pressure coefficient, $c_{p,\text{blower}}$.

Table 2. Total Power Coefficient for Example Tunnel Design

Total Power Coefficient $c_{P,\text{total}}$	
Inviscid	76.80
Viscous	91.73

Insight into the boundary layer is provided in Figure 11 where the shape factor H and non-dimensional kinetic energy defect are plotted along the length of the tunnel.

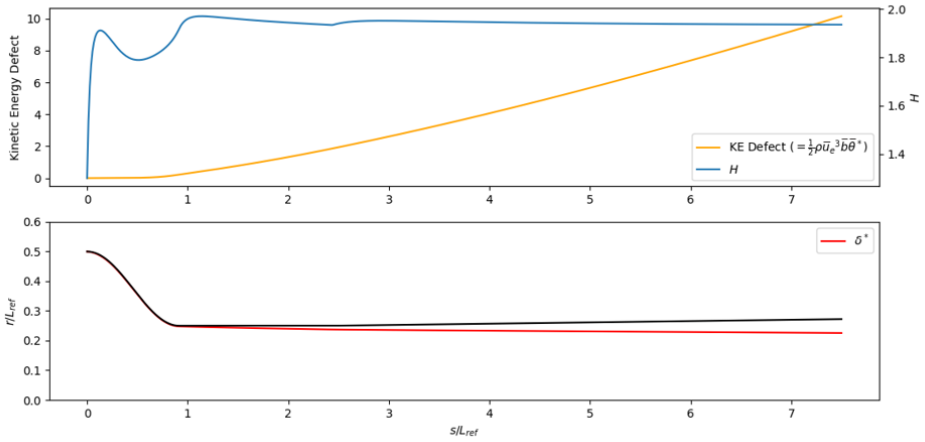

Figure 11. Boundary Layer Parameters for Example Design

The shape factor H, after quickly adjusting to a new initial value, generally decreases in favorable pressure gradients and increases in adverse pressure gradients. In this case, the shape factor decreases through the diffuser since the increase in displacement thickness overcomes the deceleration of the diffuser. Still, the shape factor H does not reach separation values of approximately 2.7 for a turbulent boundary layer [14]; this is expected since the area ratio of the diffuser AR_{diff} is small enough to avoid stall. Additionally, the non-dimensionalized kinetic energy defect is plotted along the length of the tunnel in Figure 11. The kinetic energy defect

describes the kinetic energy flow lost to the effects of viscosity within the boundary layer. This lost power requires additional power from the fans and so it is desirable to reduce the kinetic energy defect when possible.

4.3 Exploring the Design Space

Continuing the conceptual design of a wind tunnel for assessing turbomachinery with non-uniform inlet flows, the tunnel performance was assessed for a range of diffuser area ratios AR_{diff} and reference (inlet) Reynolds numbers Re_{ref}. This procedure was done for three different fan diameters d_{fan}: 12 inches (0.3048 meters), 18 inches (0.4572 meters), and 24 inches (0.6096 meters). In this analysis, the diffuser area ratio AR_{diff} was varied from 0.5 to 2. For diffuser area ratios more than 2, flow separation is likely and the assumptions underlying the governing equations in Chapter 2 no longer apply. The reference Reynolds number was varied from 100,000 to 2,000,000. Designs were assessed in terms of $Re_{\text{test}} = \frac{u_{\text{test}} d_{\text{fan}}}{\nu}$ and total power.

Using this technique, a diffuser area ratio and fan diameter can be found which maximize the test Reynolds number Re_{test} for a given power constraint of 300 horsepower (220,650 Watts). The goal was to match the test Reynolds number to Reynolds numbers up to 7 million, which are similar to those experienced by commercial turbofans in flight. The wind tunnel designs presented in this analysis could not reach those values, so instead the goal was to maximize the test Reynolds number. The diffuser decelerates the flow before it reaches the blower fan, however for large diffuser area ratios the viscous losses due to the boundary layer growth may offset this benefit. In the case where the pressure coefficient is far above zero due to the test fan, a nozzle can be used to reduce the pressure before the throttle at the exit. Since the components and sections need to be separated by lengths of the same order as the fan diameter

d_{fan}, the smaller fan diameter allows for a longer diffuser, whereas the larger fan diameter increases the test section but decreases the diffuser length. Additional diffuser length can be beneficial to reduce the adverse pressure gradient by extending the length over which the flow decelerates, however the additional wetted area promotes the development of the boundary layer and the resulting viscous losses. For this reason, it can be beneficial to truncate the tunnel diffuser area earlier; this is not explored in this analysis.

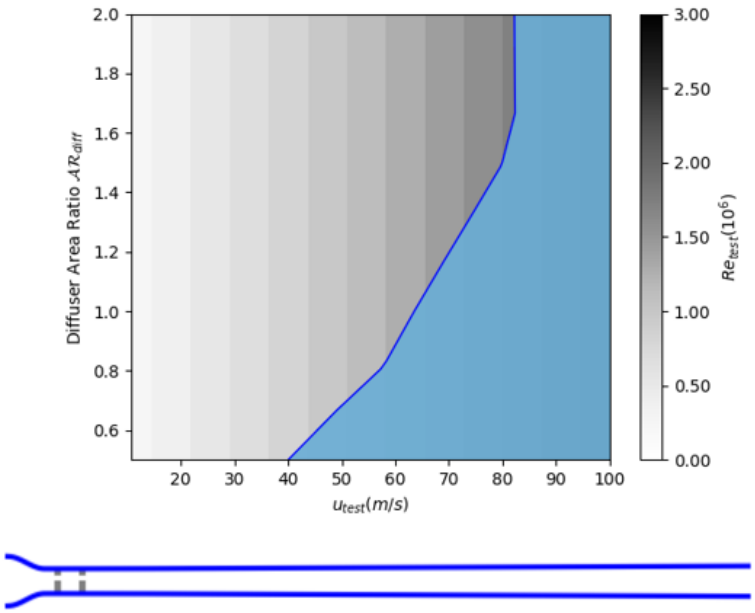

Figure 12. Design Space Results for Small Fan (12 in.)

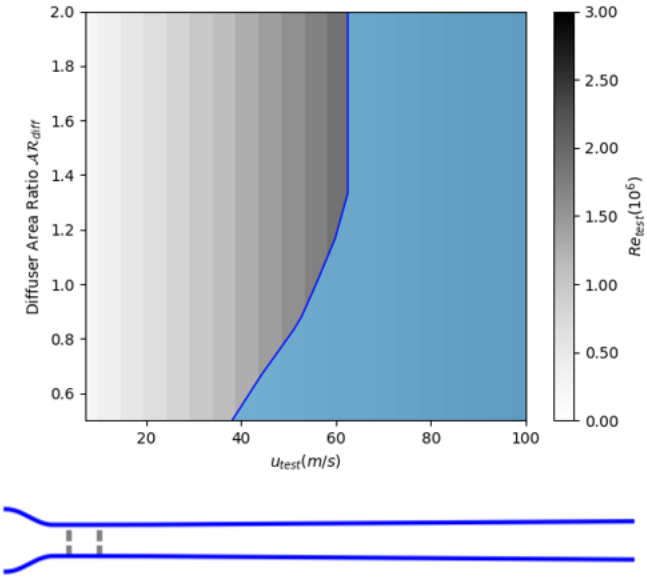

Figure 13. Design Space Results for Medium Fan (18 in.)

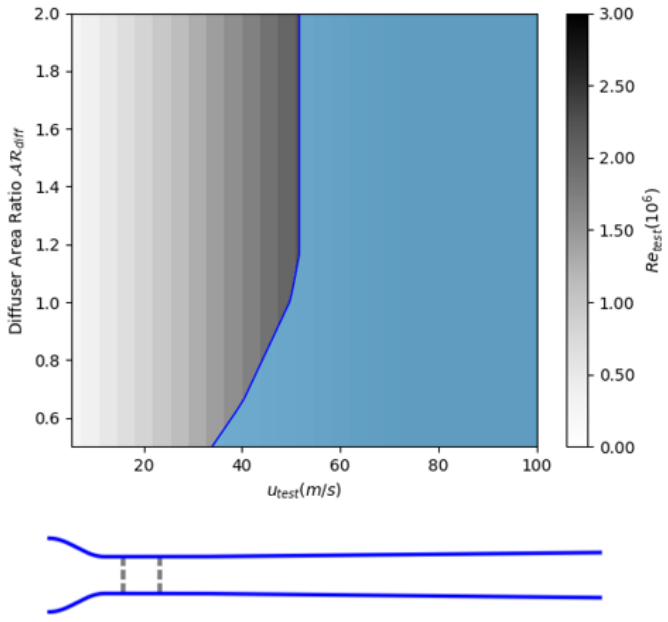

Figure 14. Design Space Results for Large Fan (24 in.)

When the diffuser area ratio is below 1, describing a nozzle instead of a diffuser, the pressure coefficient reduces to below zero at the exit, requiring a blower fan to increase the pressure. The result is higher pressure requirements at these area ratios, as depicted by the curve in the shaded blue region in Figures 12-14. Once the diffuser area ratio is above the value where a blower fan is required, the 300-hp pressure constraint becomes nearly vertical since the throttle does not require power input. Still, greater diffuser area ratios promote boundary layer growth, and so the "optimal" design point is at the intersection of these two regimes where the exit pressure coefficient is approximately zero.

The preliminary results indicate a maximum test Reynolds number of 2.06 million for the wind tunnel with the 24-inch fan diameter at a diffuser area ratio of 1.06. The tunnel with the large fan diameter (24 in) provides a balance the combination of test section velocity and diameter which provides the greatest test Reynolds number.

Chapter 5

Conclusion

In this thesis, a quasi-one-dimensional, viscous-inviscid approach was presented for the assessment of low-speed wind tunnel designs. The inviscid model relates the geometry of the tunnel to changes in velocity and pressure. The viscous model couples an inviscid core flow to the numerical integration of the axisymmetric boundary layer equations, allowing for insight into the viscous effects generated by the boundary layer. The boundary layer was assumed turbulent for the high Reynolds numbers in the tunnel and the turbulent closure model was provided from reference [10]. Models were presented for two fundamental wind tunnel components: the screen and the fan. A *k*-model was used to model the pressure drop across the screen. The pressure rise across an ideal fan was described using a design pressure rise coefficient ψ and flow coefficient ϕ. The equations of motion were arranged for numerical integration which was performed with the SciPy solve_ivp package.

The approach was applied to the conceptual design of a notional wind tunnel geometry with which to assess turbomachinery performance with non-uniform inlet flows. The design space was parameterized such that the tunnel geometry could be described using a small number of parameters. For a provided inlet reference Reynolds number, the test Reynolds number and power required were solved for. By sweeping across varying inlet Reynolds numbers and diffuser area ratios for three different fan diameters, it was determined that the large fan diameter (24 in), provided the highest test Reynolds number of 2.06 million at a diffuser area ratio of 1.06 for a power constraint of 300 horsepower.

The current analysis applies to low-speed, open-circuit wind tunnels. Future work might extend the approach to incorporate compressibility effects or the capability of assessing closed-circuit tunnel designs. Additionally, screens have an upstream influence and boundary layer thinning effect described by reference [15] which was not included in the screen model presented; the fan model might be extended to include off-design conditions. More component models may be added such as heat exchangers or turning vanes. Also, more design variables might be added to provide a more detailed description of the tunnel geometry. Finally, future work might approach the design space exploration as an optimization problem with the goal of maximizing the test Reynolds number by varying the diffuser area ratio, fan diameter, and inlet Reynolds number.

BIBLIOGRAPHY

[1] Barlow, J. B., Rae, W. H., and Pope, A., *Low-Speed Wind Tunnel Testing*, 3rd ed., Wiley, New York, 1999.

[2] Bradshaw, P., and Pankhurst, R. C., "The Design of Low-Speed Wind Tunnels," *Progress in Aerospace Sciences*, Vol. 5, pp.1-69, 1964.

[3] Hall, K. D., Huang, A. C., Uranga, A., Greitzer, E. M., Drela, M., and Sato, S., "Boundary Layer Ingestion Propulsion Benefit for Transport Aircraft," *Journal of Propulsion and Power*, Vol. 33, No. 5, 2017.

[4] Florea, R. V., Matalanis, C., Hardin, L. W., Stucky, M., and Shabbir, A., "Parametric Analysis and Design for Embedded Engine Inlets," Journal of Propulsion and Power, Vol. 31, No. 3, pp.843–850, 2015.

[5] Anderson, J., *Fundamentals of Aerodynamics*, 6th ed., McGraw-Hill Education, New York, 2017.

[6] Hill, P., and Peterson, C., *Mechanics and Thermodynamics of Propulsion*, 2nd ed., Addison-Wesley Publishing Company, Inc., 1992.

[7] Greitzer, E. M., Tan, C. S., and Graf, M. B., *Internal Flow: Concepts and Applications*, Cambridge University Press, Cambridge, 2004.

[8] Schlicting, H., *Boundary Layer Theory*, 9th ed., Springer, Berlin, 2017.

[9] Drela, M., *Flight Vehicle Aerodynamics*, MIT Press, Cambridge, 2014.

[10] Drela, M., and Giles, M. B., "Viscous-Inviscid Analysis of Transonic and Low Reynolds Number Airfoils," *AIAA Journal*, Vol. 25, No. 10, pp.1347-1355, 1987.

[11] Virtanen, P., Gommers, R., Oliphant, E. T., et al., "SciPy 1.0: Fundamental Algorithms for Scientific Computing in Python," *Nature Methods*, Vol. 17, No. 3, pp.261-272, 2020.

[12] Runge, C. D. T., “Ueber die Numerische Auflösung von Differentialgleichungen,” *Mathematische Annalen*, Springer, Vol. 46, No. 2, pp 167-178, 1895.

[13] Kutta, M. "Beitrag zur näherungsweisen Integration totaler Differentialgleichungen," *Zeitschrift für Mathematik und Physik,* Vol. 46, pp 435-453, 1901.

[14] Titchener, Neil, Colliss, and Babinsky. “On the Calculation of Boundary-Layer Parameters from Discrete Data,” *Experiments in Fluids,* Vol. 56, No. 8, 2015.

[15] Mehta, D. R., “The Aerodynamic Design of Blower Tunnels with Wide-Angle Diffusers,” *Progress in Aerospace Sciences*, Vol. 18, pp. 59-120, 1979.

ACADEMIC VITA

John B. Boerchers

jbb48@psu.edu • linkedin.com/in/john-boerchers-68008119a

EDUCATION:

The Pennsylvania State University, Schreyer Honors College, University Park, PA **Spring 2022**
B.S. in Aerospace Engineering

WORK EXPERIENCE:

Luxfer Magtech, Tamaqua, PA **May 2021 – August 2021**
Engineering Co-op

- Owned and created piping and instrumentation diagrams (P&ID) for each gas system and established directory to find individual part information.
- Performed technical analysis and selected components for project which reduced hazardous waste production by 60% and cut costs by approximately $5100 per run week.

RESEARCH EXPERIENCE:

Dr. Hall's Aircraft Propulsion Research Group, University Park, PA **May 2021 – Present**
Undergraduate Research Assistant

- Developing computational tool to create quasi-1D model of the flow field within provided wind tunnel geometry as part of an undergraduate thesis

Dr. Yetter's High Pressure Combustion Lab, University Park, PA **November 2019 – May 2021**
Undergraduate Research Assistant

- Implemented and applied an existing python script to efficiently determine time of laser application and mean time to ignition using optimization techniques
- Communicated weekly progress via PowerPoint presentations to collaborating students and faculty
- Designed and managed 10.6 µm infrared laser ignition experiments to quantify energy input necessary for ignition and flame propagation in experimental solid propellant

EXTRACURRICULARS:

Penn State Lunar Lion, University Park, PA **September 2018 – August 2020**
Propulsion Team Member and Test Technician

- Conducted preliminary analysis for design of a pintle injector for a pressure fed, 800lbf, liquid, bi-propellant rocket engine
- Tested pressure-fed, monopropellant, hydrogen peroxide engine on a static test stand
- Performed material treatment and passivation for plumbing used on engine test stand

AWARDS:

Evan Pugh Scholar Award
The President Sparks Award
The President's Freshman Award
Richard W. Leonhard Scholarship